Differences in the Region- and Depth-Dependent Microstructural Organization in Normal Versus Glaucomatous Human Posterior Sclerae

Forest L. Danford,[1] Dongmei Yan,[1] Robert A. Dreier,[2] Thomas M. Cahir,[2] Christopher A. Girkin,[3] and Jonathan P. Vande Geest[1,2,4,5]

[1]Department of Aerospace and Mechanical Engineering, University of Arizona, Tucson, Arizona
[2]Department of Biomedical Engineering, University of Arizona, Tucson, Arizona
[3]Department of Ophthalmology, University of Alabama School of Medicine, Birmingham, Alabama
[4]The BIO5 Institute, University of Arizona, Tucson, Arizona
[5]GIDP Biomedical Engineering, University of Arizona, Tucson, Arizona

Correspondence: Jonathan P. Vande Geest, Soft Tissue Biomechanics Laboratory, Aerospace and Mechanical Engineering, 1130 N. Mountain Avenue, Tucson, AZ 85721; jpv1@email.arizona.edu.

Submitted: April 19, 2013
Accepted: October 10, 2013

Citation: Danford FL, Yan D, Dreier RA, Cahir TM, Girkin CA, Vande Geest JP. Differences in the region- and depth-dependent microstructural organization in normal versus glaucomatous human posterior sclerae. *Invest Ophthalmol Vis Sci.* 2013;54:7922–7932. DOI:10.1167/iovs.13-12262

Purpose. This study quantitatively investigated differences in the regional- and depth-dependent human posterior scleral microstructure in glaucomatous (G) and nonglaucomatous (NG) donors.

Methods. Twenty-five posterior poles from six G and seven NG donors were analyzed using small angle light scattering (SALS) to investigate the organization of scleral fibers around the optic nerve head. Eccentricity (Ecc), fiber splay (FS), and percent equatorial fibers (PEF) were quantified.

Results. Regional statistically significant differences between G and NG groups existed in Ecc ($P < 0.0001$), FS ($P < 0.005$), and PEF ($P < 0.005$). Distinct and substantial variation through the depth occurred in all three end points. Region-specific differences in Ecc existed at the episcleral surface; however, by 40% into the depth, all regions converged to a similar value. Fiber splay increased in all regions by an average of 0.14 from the episcleral surface to the intraocular surface. The percentage of equatorial fibers decreased universally through the depth from approximately 61% to 33%. Generally, the inferior and superior regions had a lower Ecc and PEF compared to the nasal and temporal regions.

Conclusions. Region and depth of the posterior sclera are important factors that should be included when comparing scleral microstructure of G and NG tissue in experimental and computational work. The dramatic changes in the depth of the sclera may represent baseline properties that affect predisposition to primary open angle glaucoma (POAG), and necessitate that further research include depth as a factor in assessing how observed structural differences contribute to or are a result of POAG.

Keywords: glaucoma, POAG, sclera, biomechanics, microstructure, human, depth, region, dependent, glaucomatous, nonglaucomatous

The current biomechanical theory of glaucoma is founded upon a wealth of evidence showing that retinal ganglion cell axons are damaged as they pass through the region of the lamina cribrosa (LC).[1–5] This region has been shown to be highly sensitive to the effect of changes in IOP,[6,7] and it is thought that locally acting forces result in deformation[8] and the characteristic excavation of optic nerve head (ONH) tissues,[5] causing damage to axons traversing the LC.[9] Because the sclera transmits the IOP-related forces and deformations to the LC, scleral mechanical properties may play an important role in primary open angle glaucoma (POAG) development. This is supported by several studies demonstrating that scleral properties have an influential role in governing the biomechanical environment of the ONH.[3,7,10–15] Our group recently demonstrated that the posterior scleral microstructure of age-matched donor tissues from those at higher risk of glaucoma (African descent) is organized in a manner that would lead to increased scleral canal expansion with increasing IOP.[15] A well-characterized understanding of the load-bearing tissues of the optic nerve and surrounding area is necessary to elucidate the mechanism through which the retinal ganglion cell axons in the optic nerve are damaged, to better understand biomechanical factors associated with individual variation in disease susceptibility, and eventually to establish clinical metrics to predict susceptibility to POAG for a given IOP.

Given this, there is a growing interest in studying the organization of the microstructure of the peripapillary sclera.[14–19] There have been several studies reporting qualitative measures of the subsurface fiber architecture[20–24] from as far back as the 1930s. Recent studies have been published that quantitatively assess the fiber architecture in the peripapillary sclera using techniques that capture the bulk orientation through the entire thickness.[16,19] However, extensive quantitative information in the literature on the collagen fiber orientation and organization as a function of the depth and the region for the entire human sclera is lacking. The purpose

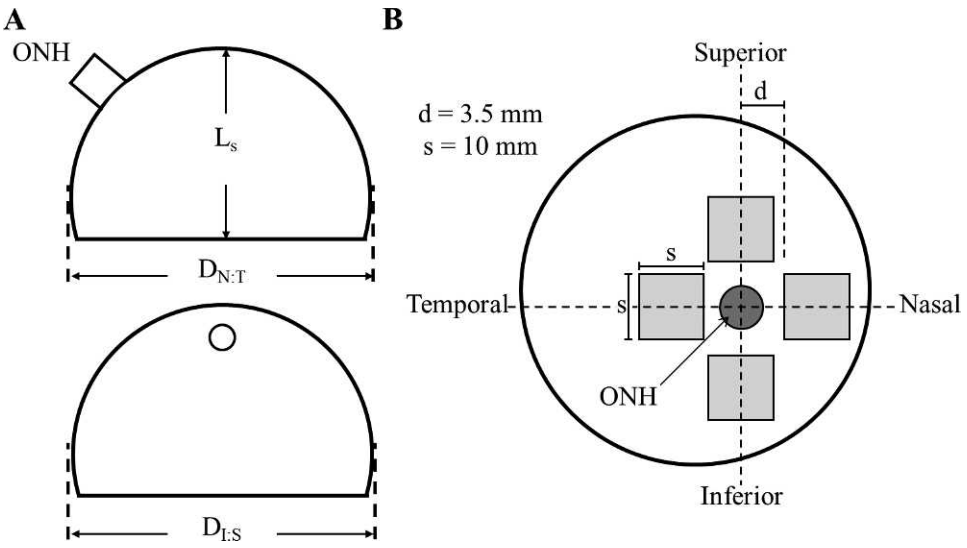

Figure 1. (**A**) Relevant physiological measurements of the posterior sclera taken before dissection. D is the average of the globe diameters $D_{N:T}$ and $D_{I:S}$, and L_s is the specimen axial length in the anterior to posterior direction. (**B**) Regional sections which were 1.0 cm^2 obtained for SALS measurement are shown in *light gray*; d is the distance from the center of the optic nerve to the start of the section, which was 3.5 mm on average. Our samples were therefore obtained from a region approximately 2.25 mm from the edge of the optic nerve.

of this study was to quantitatively investigate if differences exist in the human posterior scleral microstructure regionally and through the depth of the sclera, and if differences in microstructure exist between donors confirmed to be glaucomatous versus those having a normal ocular history.

Methods

Twenty-five donor poles from 13 donors were acquired from the Cleveland Eye Bank (CEB). We confirm that our research adhered to the tenets of the Declaration of Helsinki, that all subjects consented to donate tissue for research purposes, and that all ethical approval to use the specimens for research purposes was obtained by the CEB. Of the six total donors designated as glaucomatous (G), three were classified based on a next of kin questionnaire and review of their hospital chart. A fellowship-trained glaucoma specialist (CAG) classified the remaining three glaucomatous eyes and the seven total nonglaucomatous eyes (NG) as such after review of donors' medical records and analysis of ophthalmological records.

Sample Preparation

The time between death and preparation at the Soft Tissue Biomechanics Laboratory (STBL; Tucson, AZ) for all samples was 3 ± 0.7 days on average. Eyes were shipped in Hanks' balanced salt solution (HBSS) on ice. Upon arrival, posterior poles were transferred to phosphate-buffered saline (PBS) at 4°C. Any loose connective or fatty tissues were removed from the scleral surface. The average globe diameter, D, was calculated to be the average of the nasal to temporal diameter and superior to inferior diameter. Both D and the specimen axial length, L_s, were measured using analog calipers (Fig. 1A).

The methods utilized herein are similar to the methods described in our previous study assessing racial differences present in the posterior human sclera. For a more detailed description of specimen processing and testing, please refer to Yan et al.[15] Briefly, square specimens approximately 1.0 cm^2 were isolated from each region of the eye (Fig. 1B), and the minimum distance from the ONH center to the sample was recorded. Square tissue samples were gently flattened while being placed in tissue-freezing medium (Triangle Biomedical Sciences, Durham, NC) and then snap frozen in liquid nitrogen. All specimens were kept at −150°C until sectioning.

Each region was then cryosectioned at 70-μm intervals through the entire thickness of the sclera and transferred onto microscope slides. The slices were dehydrated and cleared in graded glycerol/water solutions (50%, 75%, 87.5%) for 30 minutes per step, and then left in 100% glycerol overnight. The glycerol was removed the following day using 100% alcohol, and a coverslip was adhered to the sample using tissue-mounting medium (Richard-Allen Scientific, Kalamazoo, MI). It is important to note that several studies have found that small angle light scattering (SALS) preparation does not significantly affect collagen fiber architecture.[15,25,26]

Small Angle Light Scattering

Small angle light scattering is a well-characterized[27] and commonly used technique to investigate soft tissue microstructure[26,28–30] based upon the preferential scattering of unpolarized HeNe laser light. During SALS experiments, laser light is scattered orthogonal to the preferred orientation of the underlying fiber architecture of the cleared and dehydrated tissue sample. The resulting light splay is captured as an image that allows for the quantification of the preferred fiber angle and degree of alignment. The SALS system utilized in this study is the same device used previously[15] and consists of a two-dimensional automated motion-controlled specimen holder, an unpolarized HeNe laser, a projection screen, and a charge coupled device camera. Light splays were generated and captured at each location (subsequently referred to as a material point) in an evenly spaced grid spanning the entire planar dehydrated sample (Fig. 2D) via a custom-written, motion-control system (LabView; National Instruments, Austin, TX). This resulted in 600 unique light splay images per slice on average, with each specimen generating approximately 16 slices.

Each light splay image was then analyzed using a built-in MATLAB function (The MathWorks, Inc., Natick, MA) to determine the local preferred fiber angle (vectors in Fig. 2E) and eccentricity (contours in Fig. 2E). The eccentricity is the ratio of the distance between the foci of the ellipse (orthogonal

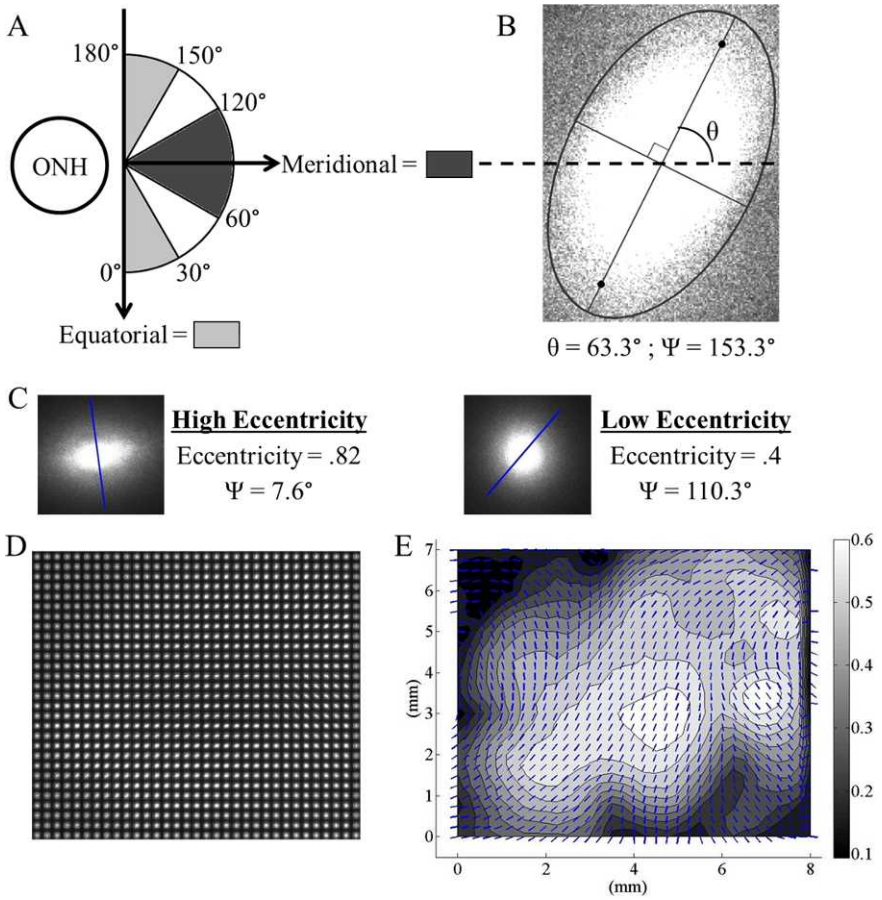

Figure 2. (**A**) The transformed polar coordinate system used in analysis and the values of Ψ corresponding to anatomical directions. (**B**) Typical SALS light splay image at a material point within a tissue slice. Ψ is the local preferred fiber angle relative to the ONH in the transformed polar coordinate system. (**C**) Two light splays at different material points representing characteristic low and high Ecc measurements. The *overlaid lines* show the local preferred fiber angles and are equivalent to the vectors in Figure 2E. (**D**) The assimilated image matrix for an entire representative slice. For a typical 10-mm^2 slice there are $\sim 29 \times 29$ unique light splays. (**E**) The corresponding vector-contour plot showing the local preferred fiber angle (overlaid vectors) and the Ecc (contour values) for the entire slice.

to the major axis in Fig. 2B) and the major axis length (at angle θ from the horizontal in Fig. 2B) as calculated from the normalized second moments of inertia of the light splay image. An eccentricity of 0 describes a perfect circle while an eccentricity of 1 describes a straight line. Correspondingly, a less organized microstructure at a material point results in a lower eccentricity because light is scattered randomly through the tissue (Fig. 2C, Min), while a highly organized microstructure at a material point results in a higher eccentricity due to preferential scattering in one direction (Fig. 2C, Max).

This process was then iteratively repeated to generate vector-contour plots for every slice from every region of the human sclera from all the samples examined in this study. The local preferred fiber angle (Ψ in Fig. 2B) was then transformed using a polar coordinate system whose origin was the ONH with the local radial direction pointing away from the ONH. Based on this system, local preferred fiber angles of 0° and 180° correspond to perfectly equatorial alignment, while a value of 90° is perfectly meridional (Fig. 2A). It is important to note that SALS does not discriminate between the collagen and elastin fibrils present in the scleral extracellular matrix. Therefore, all the quantified end points are based on the composite fiber architecture as opposed to just the collagenous microstructure. However, given the distance from the ONH at which specimens were obtained (shown in Fig. 1B), elastin fibrils are likely present only at the inner scleral surface, close to the choroid.

Quantitative End Points

The local preferred alignment of fibers in the equatorial direction (as quantified by the percent equatorial fibers or PEF), eccentricity (Ecc), and fiber splay (FS) were chosen as the end points to quantitatively assess scleral microstructure and organization. Based on the polar coordinate system used, we quantified the local preferred fiber angle as being either equatorial, conservatively defined as 0° to 30° or 150° to 180°, or nonequatorial (30°–150°) (Fig. 2A). To generate a single metric of fiber orientation for each entire slice that could be used for comparing the independent variables of side, depth, location, and group (G versus NG), we measured the local fiber angle at each material point and recorded the overall percentage of local equatorial fiber alignment for the entire slice as the PEF end point. This was done for every slice present in every sample. Given that the preferred fiber angle range that defines our equatorial bin (a total of 60°) consists of less than 50% of the total possible preferred fiber angles (which is 180°), a value of PEF >50% represents a slice with high equatorial alignment. Similarly, Ecc was calculated as an average of every light splay's Ecc in each entire slice. The fiber splay (FS) quantifies the overall variability of the preferred fiber

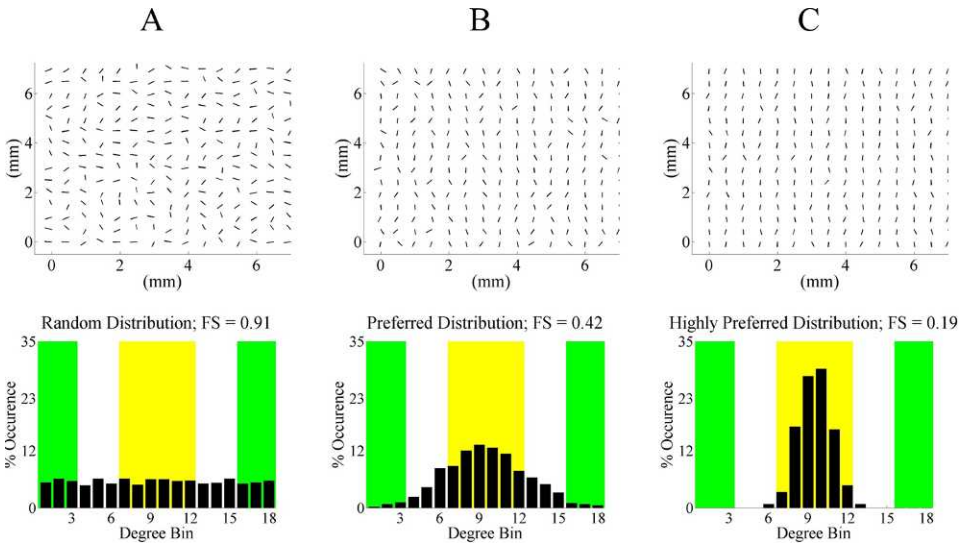

Figure 3. Vector plots of local preferred fiber angles and their corresponding histograms for three hypothetical cases to illustrate the possible values of FS. The *green ranges* indicate equatorial alignment, and the *yellow range* represents meridional alignment. Note that all bar graph values in each distribution add up to 100% because the end point is normalized to the total number of light splays analyzed in the tissue slice. (**A**) No preferred orientation, resulting in an FS ≈ 1. (**B**) Preferred fiber angle orientation. (**C**) Highly preferred fiber angle orientation with an FS smaller than (**B**).

angle orientations within 10° bins (0°–10°, 10°–20°, and so on to 180°) for each slice using the following equation:

$$FS = \frac{\sum_{i=1}^{N} \frac{b_i}{b_{max}}}{N} \quad (1)$$

where N is the total number of bins created for the local preferred fiber angle (18 for 10° bins), b_i is the number of light splays in angle bin i, and b_{max} is the number of light splays in the local preferred fiber angle mode.

Equation 1 provides a similar but more robust sense of the variability of preferred angle as compared to a metric such as the full width at half-maximum[31] because it is able to quantify multimodal systems. Fiber splay is also distinct from Ecc as it measures dispersion on a different length scale. Eccentricity measures the preference of local alignment at a material point as opposed to FS, which measures the preference of alignment for the entire 1-cm^2 sample. The FS end point is between 0 and 1, where an FS close to 0 represents a sample having a highly preferred distribution (Fig. 3C) and an FS of 1 represents a randomly oriented sample (Fig. 3A). The correlation between the vector plot, the local preferred fiber angle distribution, and the resulting FS value is illustrated in Figure 3.

In order to account for the variability in the number of slices per sample, all end points were binned into 10 groups based on the percent depth from the episcleral surface to the inner sclera they represented; that is, depth bin 1 is outermost scleral surface to 10% of the total depth, and depth bin 10 is 90% of the depth to the innermost scleral surface analyzed. A vast majority of bins included multiple slices. Thus binned values were determined by weighting the variable based on the number of light splays present in the slices using the following equation:

$$Var^* = \sum_{i=1}^{N} \frac{b_i}{\tau} * (Var_i) \quad (2)$$

where Var^* is the binned value of the variable being quantified

Table 1. Clinical and Demographic Information Used for Donor Samples

Donor ID	Age	Sex	Race/Ethnicity	Clinical Record Info
G1	75	M	Caucasian	Visual field, C/D, HRT
G2	68	M	Caucasian	IOP, C/D
G3	76	F	Caucasian	IOP, C/D
G4	74	M	Caucasian	Visual field, retinal nerve fiber thickness
G5	74	M	Caucasian	Next of kin questionnaire and review of hospital record
G6	75	F	Caucasian	Next of kin questionnaire and review of hospital record
N1	51	M	Caucasian	Visual field
N2	49	M	Caucasian	IOP
N3	35	M	Caucasian	IOP, C/D
N4	47	F	Caucasian	Visual field
N5	22	M	Caucasian	Ophthalmological history
N6	52	M	Caucasian	IOP
N7 (L pole only)	75	M	Caucasian	C/D, IOP

Summary of the demographic and clinical information available for the 13 donors used in the study. Donors who were confirmed to be glaucomatous ($n = 6$) are indicated as such by "G," while those confirmed to have a normal ocular history ($n = 7$) are indicated as such by "NG." C/D, cup-to-disc ratio; HRT, Heidelberg Retinal Tomograph.

Investigative Ophthalmology & Visual Science

Table 2. Age, Race, and Sex as a Function of Ocular History

	Age			Sex	
	0–30	30–60	60+	Male	Female
G	0	0	8	5	3
NG	1	5	2	7	1

Distribution of age, race, and sex of the donor samples with respect to ocular history.

(Ecc, PEF, FS), N is total number of slices in that bin, h_i is number of light splays in slice i, τ is total number of light splays being placed in that bin, and Var_i is value of variable of interest for slice i.

Statistical Analysis

One-sample Kolmorgorov-Smirnov tests were used to determine the normality of the data for the three end points Ecc, FS, and PEF. Based on the Kolmorgorov-Smirnov tests, all of the end points with the exception of the fiber splay rejected the null hypothesis at a significance level of $\alpha = 0.05$. A Box-Cox transformation was then utilized to normalize the data so that statistical analyses of the independent variables and between interactions of independent variables could be performed using a commercial statistical software package (SAS software version 9.3; SAS Institute, Inc., Cary, NC). A repeated measures ANOVA was chosen to evaluate the significance of the following independent variables in each end point: side (left and right), depth (1–10), region of pole (superior, inferior, and so on), and group (G and NG). The statistically significant interactions from the ANOVA analysis are summarized in Table 3.

All of the graphical data are presented using error bars equal to the standard error of the measurement. The mean values and standard errors in the case of Ecc and PEF are back-calculated from the Box-Cox transformed data (Box-Cox transformed mean and Box-Cox transformed distribution, respectively). Post hoc analyses consisting of Student's *t*-tests with Bonferroni correction were performed to compare specific mean values of significant interactions. Paired Student's *t*-tests with Bonferroni correction were performed to compare values within an independent variable in the case of two-way interactions. The Bonferroni correction method was chosen as it is the most conservative method to account for family-wise error rate.

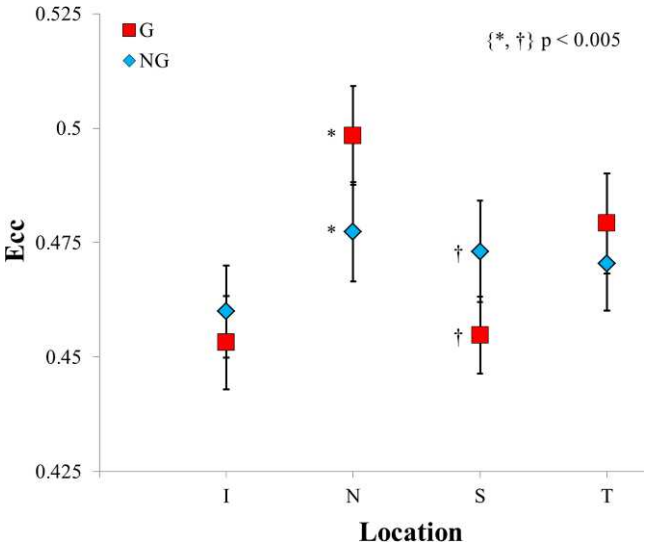

Figure 4. A comparison of the glaucomatous and nonglaucomatous groups' eccentricities as a function of region on the posterior sclera. Due to the large number of statistically significant differences, the within-group markers have been omitted (please refer to the text for these omitted results).

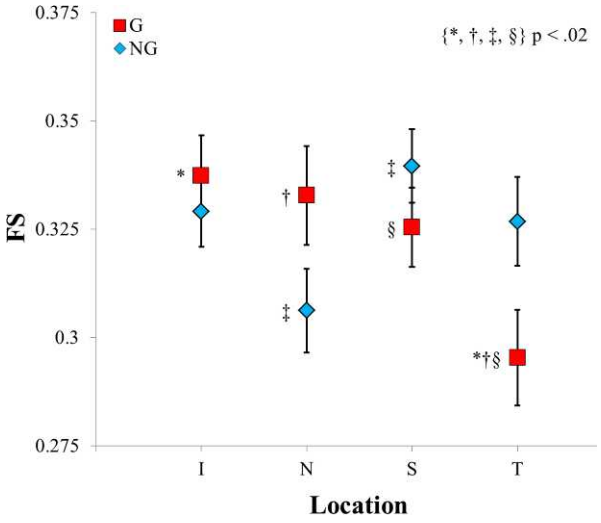

Figure 5. A comparison of the glaucomatous and nonglaucomatous groups' FS binned means as a function of region on the posterior sclera.

Results

The mean globe diameter of the posterior scleral shells (D in Fig. 1A) was 24.2 ± 0.61 mm for the glaucomatous samples and 24.0 ± 1.04 mm for the nonglaucomatous samples ($P >> 0.05$). The mean axial length (L in Fig. 1A) was 19.4 ± 0.96 mm for the glaucomatous samples and 19.1 ± 0.72 mm for the nonglaucomatous samples ($P >> 0.05$). As such, the geometries of the two groups were not significantly different and therefore were not further investigated in this study. The average distance from the center of the ONH to the scleral samples (d) was 3.4 ± 0.9 mm. The relevant donor demographic information is presented in Tables 1 and 2.

There were significant interactions between the independent variables of side, depth, location, and group (G versus NG). Age and sex were not significant factors with respect to any of the end points. Interestingly, side was a statistically significant factor in at least one interaction in all three end points. The largest-magnitude difference was 0.032 in PEF in the glaucomatous left versus glaucomatous right eyes. The difference in PEF between the nonglaucomatous left and right eyes was very similar at 0.031. However, the only instance in which differences in side were statistically significant occurred in Ecc in the temporal region ($P < 0.005$). In this instance, both the glaucomatous and nonglaucomatous temporal left sides had a higher Ecc than the right sides.

Statistical differences are displayed using standard symbols; however, in the interest of clarity, some figures have only selected significances designated. In these instances, the related text discusses the statistically significant but unmarked differences.

Region-Dependent Differences in Glaucomatous Versus Nonglaucomatous Samples

Eccentricity. The mean Ecc values for the G group were 0.45 ± 0.01, 0.50 ± 0.01, 0.45 ± 0.01, and 0.48 ± 0.01 for the inferior (I), nasal (N), superior (S), and temporal (T)

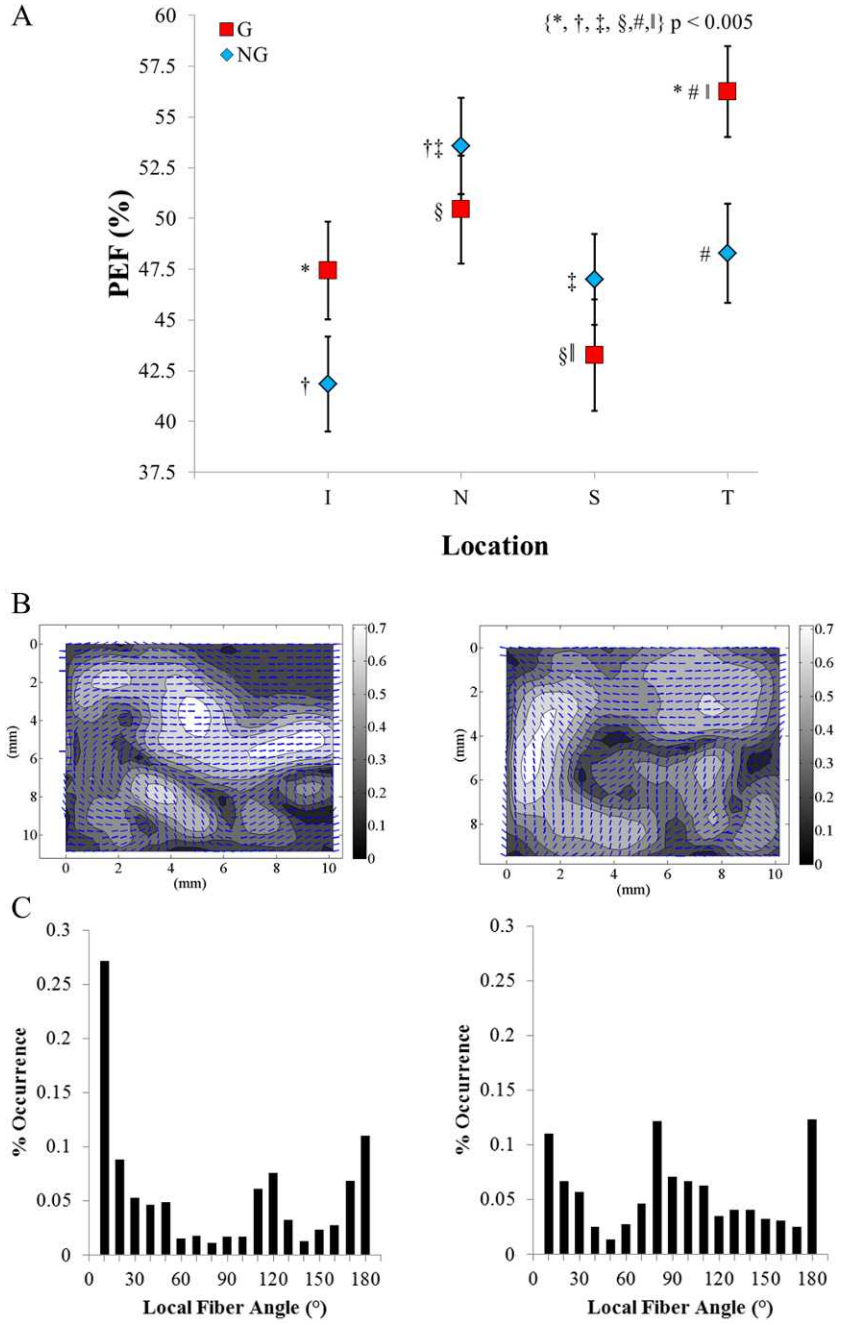

Figure 6. **(A)** A comparison of the glaucomatous and nonglaucomatous groups' PEF binned means as a function of region on the posterior sclera. **(B)** Representative vector-contour plots from depth bin 2 of the left temporal region from glaucomatous donor G4 and nonglaucomatous donor N5. The overlaid vectors show the local preferred fiber direction, and the contour values show the local Ecc. **(C)** The distribution of local fiber angles used to calculate the PEF. The PEF in G4 was 64.4%, as compared to a PEF of 44.6% for N5.

regions, respectively. The NG group's mean eccentricities were 0.46 ± 0.01, 0.48 ± 0.01, 0.47 ± 0.01, and 0.47 ± 0.01 for the I, N, S, and T regions, respectively. The two-way interaction of the disease state and region for Ecc was significant at $P < 0.0001$. Based on the post hoc analysis, the Ecc was significantly different for the nasal and superior regions. The mean Ecc in the G group was greater than in the NG group in the nasal region and less than in the NG group in the superior region ($P < 0.005$ for both). The data then suggest that in normal scleral tissue, the superior region is more highly organized than in glaucomatous scleral tissue. Conversely, in the nasal region, the glaucomatous group's scleral tissue is more highly organized compared to normal scleral tissue.

Within the G group, the nasal and temporal regions had significantly larger eccentricities than either the inferior or superior region ($P < 0.000005$). There was no statistical difference between the inferior and superior regions within the G group. This is in comparison to the NG group, in which only the inferior region was significantly different from any other region ($P < 0.01$ for inferior versus nasal and superior). Figure 4 summarizes the above results.

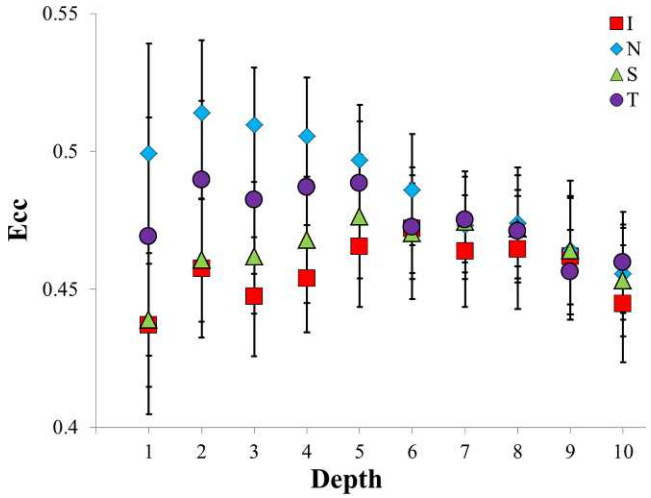

FIGURE 7. A comparison of regional variations in Ecc as a function of depth in the posterior sclera. Statistically significant differences occurred at depths 1, 2, 3, and 4. Statistically significant differences within regions exist, but are not shown.

Fiber Splay. The mean FS values for the G group were 0.34 ± 0.01, 0.33 ± 0.01, 0.33 ± 0.01, and 0.30 ± 0.01 for the I, N, S, and T regions, respectively. The NG group's mean values for FS were 0.33 ± 0.01, 0.31 ± 0.01, 0.34 ± 0.01, and 0.33 ± 0.01 for the I, N, S, and T regions, respectively. The two-way interaction of the G group versus the NG group for FS was significant at $P < 0.005$. Based on the post hoc analysis, the FS approached significance only in the temporal region, with the NG group having a larger FS than the G group ($P < 0.05$).

Within the G group, the temporal region had a significantly smaller FS than the inferior, nasal, and superior regions ($P < 0.0125$ for all). Within the NG group, the superior region had a significantly larger FS than the nasal region ($P < 0.005$). Figure 5 summarizes the above results.

Percent Equatorial Fibers. The mean PEF values for the G group were 47% ± 2.4%, 50% ± 2.7%, 43% ± 2.8%, and 56% ± 2.2% for the I, N, S, and T regions, respectively. The NG group's mean PEF were 42% ± 2.3%, 54% ± 2.4%, 47% ± 2.2%, and 48% ± 2.4% for the I, N, S, and T regions, respectively. The two-way interaction of the G group versus NG group by region for PEF was significant at $P < 0.005$. Based on the post hoc analysis, the PEF was significantly different in the temporal region ($P < 0.005$) and approached significance in the inferior region ($P < 0.05$). In both cases, the G group had a larger PEF than the NG group.

Within the G group, the superior region had a significantly smaller PEF than the nasal and temporal regions ($P < 0.005$ for both). Additionally, the temporal region was significantly larger than the inferior region ($P < 0.0005$). Within the NG group, the nasal region had a significantly larger PEF than both the inferior and superior regions ($P < 0.005$). The difference between the nasal and temporal regions was less pronounced and approached significance at $P < 0.05$. Figure 6 summarizes the above results.

Region-Dependent Differences in the Depth of the Sclera

Eccentricity. The two-way interaction of region and depth for Ecc was significant at $P < 0.005$. From the episcleral surface through 40% of the depth of the samples, differences between regions were statistically significant. At the episcleral surface, the nasal region was greater than both the inferior and superior regions ($P < 0.01$ for both; approximately a 0.06 magnitude difference). Depths 2 and 3 had similar regional differences, but at depth 4, the differences became less pronounced. By depth 5, all of the regions, regardless of the region-specific starting Ecc, converged to an average Ecc of approximately 0.47 and stayed relatively close to this value through the remainder of the depth.

The nasal region started at a value of 0.5, increased to 0.51 in bin 2, and then decreased continuously to a final Ecc of 0.46. Generally these early depths for all regions were significantly larger than the deeper depths; depths 2 through 5 were significantly different from depths 7 through 10 ($P < 0.005$), with the exception of depth 5 compared to depth 8. The inferior region started at 0.44, gradually increased to a peak of 0.47 at depth 6, and then decreased continually to 0.44. The superior and temporal regions exhibited similar, albeit milder, behavior. These three regions had few depths that were significantly larger or smaller than any other depths in the respective region. The above results are summarized in Figure 7 and Table 4.

Fiber Splay. The interaction of location and depth for FS was significant at $P < 0.0001$. As one moves from the episcleral surface to the inner surface of the sclera, the FS increased continuously in all regions except for the superior until depth 9, at which point all regions except for the temporal experienced a small decrease. On average, the FS increased by 0.14 from the episcleral surface to the retinochoroidal inner surface.

In the superior region, the FS increased steadily from 0.24 to 0.4 until depth 6, at which point an abrupt drop occurred, resulting in an FS similar to the final FS values of the inferior and nasal regions. Compared to the other regions, the FS in the inferior region increased more gradually from 0.28 to 0.37 until depth 6, at which point it stayed constant. The FS in the nasal region increased steadily from 0.19 until depth 4, where it experienced an abrupt increase to 0.33, continued increasing steadily until bin 9, and then dropped from 0.4 to 0.36. The temporal region FS increased steadily from 0.2 at depth 1 to 0.42 at depth 10. It can be observed in Figure 3 that changing the FS from 0.17 to 0.42 results in a dramatically different local

TABLE 3. Statistically Significant Differences by End Point

Ecc		FS		PEF	
Independent Variable	***P* Value**	**Independent Variable**	***P* Value**	**Independent Variable**	***P* Value**
Location	<0.0001	Side	0.0099	Location	<0.0001
Depth	<0.0001	Depth	<0.0001	Depth	<0.0001
Location × group	<0.0001	Location × group	0.0029	Location × group	0.0010
Location × depth	0.0019	Location × depth	<0.0001	Location × depth	0.0020
Side × location	0.0001			Side × group	0.0297
Side × group	0.0250				

All statistically significant interactions as identified by the repeated measures ANOVA (three- and four-way interactions exist, but are not shown).

Investigative Ophthalmology & Visual Science

Table 4. Statistically Significant Depth-Dependent Differences in Ecc

Depth	Result
1	N > S
	N > I
2	N > S
	N > I
3	N > S
	N > I
4	N > S
	N > I
	T > I

A summary of the statistically significant depth-dependent differences in Ecc; all differences listed are $P < 0.01$ (see Fig. 7).

preferred fiber angle distribution. The above results are summarized in Figure 8 and Table 5.

Percent Equatorial Fibers. The interaction of location and depth in PEF was significant at $P < 0.005$. As one moves from the episcleral surface through the depth, the PEF decreased substantially in all groups. Both the nasal and superior regions showed a steady decrease in PEF (nasal: PEF depth 1 = 0.74, PEF depth 10 = 0.35; superior: PEF depth 1 = 0.67, PEF depth 10 = 0.29), while the temporal and inferior regions stayed relatively constant at a PEF of 0.52 and 0.55, respectively, until depth 4, and then decreased steadily through the remainder of the depth. On average, the PEF decreased from 0.61 to 0.33 from the episcleral surface to the retinochoroidal inner surface. The above results are summarized in Figure 9 and Table 6.

Discussion

Our results demonstrate that statistically significant regional differences exist in the microstructural organization of G versus NG groups. The NG group had a higher Ecc than the G group in the superior region, while the G group had a higher Ecc in the nasal region. Generally, the G group had more intergroup regional variation when compared to the NG group. The changes in all end points in the depth-dependent interactions were dramatic. We found that the Ecc was greater and initially region specific, but converged to a lower, region-independent value by 40% of the total thickness of the sclera through the remainder of the depth. The nasal and temporal regions reached their peak Ecc values simultaneously in depth bin 2, while the inferior and superior regions reached their peak Ecc values deeper into the sclera at bins 6 and 5, respectively. The FS increased substantially as one moves from the episcleral surface (depth 1 $\approx$ 0.23, Fig. 7) to the inner scleral surface (depth 10 $\approx$ 0.37, Fig. 7). The PEF showed the exact opposite trend, having significantly more equatorially aligned fibers on the episcleral surface (depth 1 $\approx$ 60%, Fig. 8) as compared to the inner surface (depth 10 $\approx$ 33%, Fig. 8). In the depth-dependent interactions, the FS and PEF appeared to be paired in the sense that as one increased, the other tended to decrease. For all end points, there was no statistical difference between the G and NG groups as a function of depth (not shown); however, the PEF value approached significance at $P < 0.06$. In both regional and depth interactions, the nasal and temporal groups generally had similar values that were different than those in the superior and inferior regions, which were also similar to each other. Given the large change that occurs through the depth of the sclera, we suggest that it would be of considerable value to include depth-dependent microstructural information in future numerical simulations looking at biomechanics of the ONH.

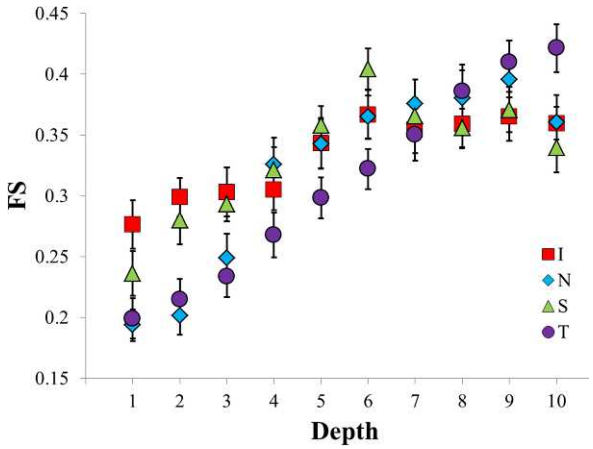

Figure 8. A comparison of regional variations in FS as a function of depth in the posterior sclera. Statistically significant differences occurred at depths 1, 2, 6, and 10. Statistically significant differences within regions exist, but are not shown.

The presented SALS results agree with the body of evidence suggesting that scleral tissue is highly inhomogeneous both regionally[16,17,19,32,33] and through its depth.[15,16,21,23] Given the limitations of previous studies investigating scleral microstructure, our results greatly expand upon the evidence suggesting that human scleral fibers are arranged in a more highly aligned pattern that is predominantly equatorial near the episcleral surface and becomes more random near the inner surface[15,16,21] (Figs. 7–9). The consistent changes observed in both the FS and PEF may be functionally important because the sclera is responsible for conferring not only rigidity to the eye, but also flexibility to compensate for acute, short-term, and long-term fluctuations in intraocular pressure.[34] The high degree of alignment (as measured by FS) in an equatorial fashion (PEF) on the outer surface may result in a more rigid and protective microstructure. Similarly, the more random distribution (as measured by FS) and lower degree of equatorial alignment (PEF) on the inner surface may allow for increased local deformation and therefore prevent damage to delicate yet critical tissues at the retinochoroidal scleral interface.

When investigating regional interactions (accomplished by averaging groups in Figs. 4–6, not shown), we found that the superior and inferior regions had fewer equatorially aligned fibers (PEF = 45% $\pm$ 2% and 44% $\pm$ 2%, respectively; $P < 0.001$) and a lower Ecc (Ecc = 0.46 $\pm$ 0.007 and 0.46 $\pm$ 0.007, respectively; $P < 0.01$) compared to the nasal and temporal regions (PEF = 52% $\pm$ 2% and 52% $\pm$ 2%, respectively; Ecc = 0.49 $\pm$ 0.007 and 0.47 $\pm$ 0.007, respectively). The PEF results support a similar observation noted by Pijanka et al.,[16] who found that in both glaucomatous and nonglaucomatous sclera there were meridional fiber bands radiating tangentially from the superior and inferior regions in superior–nasal and inferior–nasal directions, respectively (Fig. 6 versus Figs. 4A–4D from Pijanka et al.[16]). Given the hypothesis that the circumferential ring of collagen fibers present in the peripapillary sclera confers protection to the LC,[12,13,22,24] it is possible that the difference in orientation and microstructural organization between these regions could be a contributing factor to the well-characterized clinical observation that the superior and inferior regions experience axon loss at a preferential rate during POAG development.[35,36] In contrast to the group and regional anisotropy findings of Pijanka et al.,[16] our Ecc results (analogous to their anisotropy measurement) indicated that there were statistically significant differences in the degree of preferred fiber angle for the areas of sclera that correspond

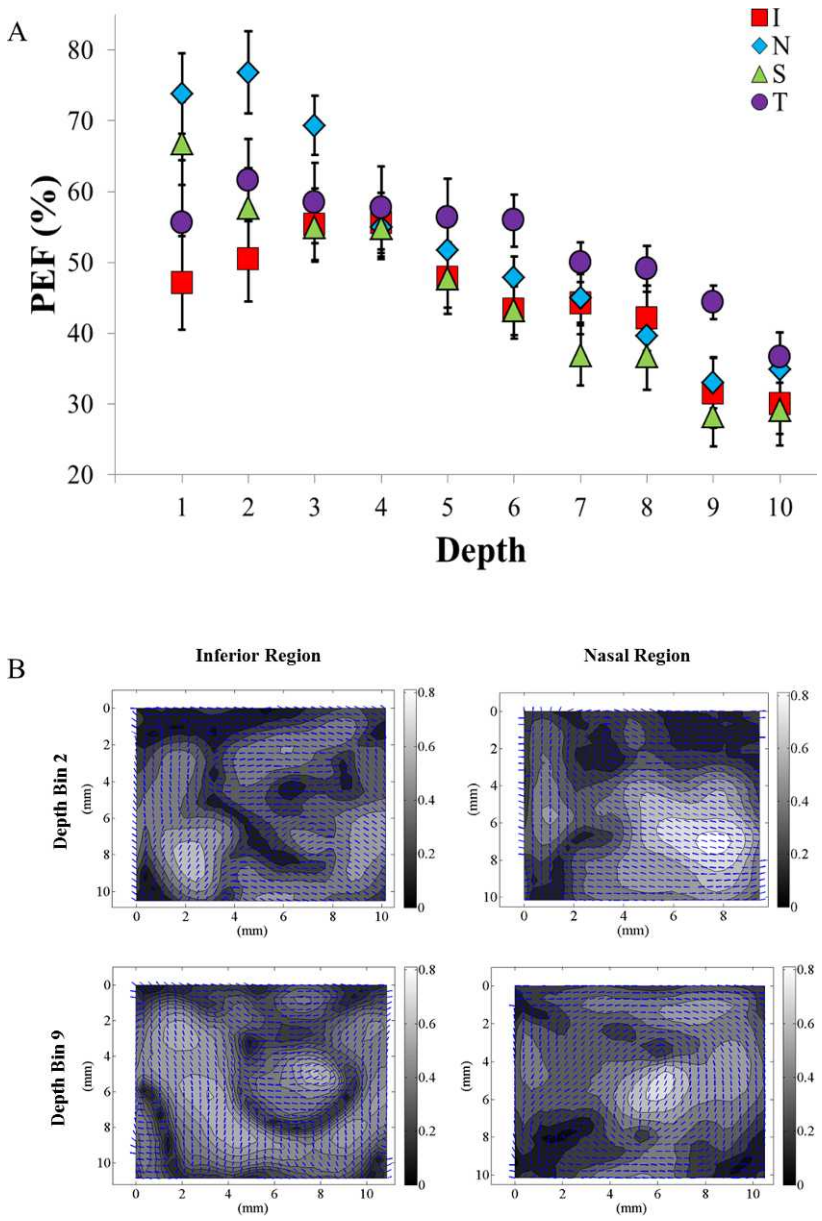

Figure 9. (**A**) A comparison of the regional variations in the PEF as a function of depth in the posterior sclera. Statistically significant differences occurred at depths 1, 2, and 6 through 9. Statistically significant differences within regions exist, but are not shown. (**B**) Representative vector-contour plots showing the regional- and depth-dependent changes. The PEF in the inferior region was 50.2% at depth bin 2 and decreased to 26.2% by depth bin 9. The PEF for the nasal region started at a much higher initial PEF of 76.5% at depth bin 2, but experienced a similar large decrease in PEF to 31.2% by depth bin 9. In all regions the PEF decreases significantly with increasing bin depth.

across studies. Our results indicated that the glaucomatous samples exhibited a greater degree of preferred fiber angle in the nasal region and a lower degree of preferred fiber angle in the superior region (as measured using Ecc, shown in Fig. 4). Additionally, our data showed that the G group had a significantly higher percentage of equatorially aligned fibers in the temporal region compared to the NG group, while Pijanka et al.[16] found that there were no notable differences between groups in their bulk fiber direction. However, several factors may make direct comparisons between the studies difficult. Firstly, the areas of the sclera analyzed were not identical. In the Pijanka et al. study, the sclera was subdivided into grouped quadrants (superior–nasal quadrant, inferior–temporal quadrant, and so on), while our scleral samples were obtained directly from the superior, nasal, inferior, and temporal regions. Secondly, the size of the area studied and the proximity to the ONH were quite different. Pijanka et al. analyzed all scleral tissue within a 6.5-mm annulus of the ONH, while our group sampled a 1-cm^2 area that started on average 2.25 mm from the edge of the optic nerve. Thirdly, different modalities were used to quantify the scleral microstructure. Additionally, it should be noted that while the Ecc region–group differences were statistically significant, the magnitudes of differences were relatively small. Further research is warranted to investigate if these small differences result in important physiologically consequences.

The results of the repeated measures ANOVA treating side as an independent variable were unexpected. Our results

Table 5. Statistically Significant Depth-Dependent Differences in FS

Depth	Result
1	I > T
	I > N
2	I > T
	I > N
	S > N
6	S > T
10	T > S

A summary of the statistically significant depth-dependent differences in FS; all differences listed are $P < 0.007$ (see Fig. 8).

Table 6. Statistically Significant Depth-Dependent Differences in PEF

Depth	Result
1	N > I
2	N > I
6	T > S
	T > I
7	T > S
8	T > S
9	T > S
	T > I
	T > N

A summary of the statistically significant depth-dependent differences in FS; all differences listed are $P < 0.01$ (see Fig. 9).

suggest that there were small differences between the Ecc in left versus right eyes in the nasal and temporal regions. These differences noted in Ecc, however, were at most ~0.03 in magnitude. We also found that the side–group interaction for PEF was significant, with the right glaucomatous eyes having a higher percentage of equatorially aligned fibers (~5% greater) as compared to the nonglaucomatous right eyes. The remaining statistically significant differences are all small in magnitude. Though the clinical information available from the donor samples indicated that the extent of glaucomatous damage was equal in both eyes, there were two donors who had not had any clinical imaging and therefore the extent of damage in the left versus right eyes was unknown. It is possible that this contributed to the observed differences in side. While there is little specific information in the literature regarding symmetry in microstructure between matched left and right eyes, Pijanka et al.[16] noted a qualitative feature conferring symmetry between eyes in their results. Ongoing analysis is being performed in our lab to identify if quantitative microstructural symmetry is present between the left and right eyes in our study.

A major weakness in the study was the lack of complete clinical data to classify glaucomatous versus normal eyes, as well as the degree of glaucomatous damage and disease status. Although we obtained detailed ophthalmological records, several of our donors had not had visual fields or other clinical tests performed that allowed for correlation of clinical information to the information gathered from the SALS experiments. While the definitions are imperfect, there is little reason to expect a differential misclassification bias between groups with fiber orientation within the sclera. Therefore, the misclassification that is present due to incomplete clinical information would bias estimate of association toward a nonsignificant result, as is the case with nondifferential misclassification. Due to this, the significant associations seen in this study likely underestimate any "true" association. In the future, our laboratory will utilize optic nerve grading via axon counts to corroborate available clinical evidence of glaucoma and better quantify regional differences and the extent of damage. This information will allow us to more directly correlate the observed regional SALS data with regional axon losses.[35] Another limitation encountered in this study was the lack of age-matched available donor tissue. Thus the normal group represents a much younger population as compared to the G group. However, our previous work, which had a relatively large sample size within each representative age group, indicated that age was not a significant factor in governing posterior scleral microstructure,[15] albeit only in the temporal region of right eyes. Additionally, statistical analysis performed during this study did not indicate that age was a significant factor in any of the end points. That being said, we did not have a large sample size across ages for our donor groups, so it would be inappropriate to make any strong conclusions regarding the effect of age from the present study. This being the case, the question of the effects of aging on scleral microstructure remains open, and it is possible that some of the observed differences between the G group and NG group may be due to the differences in the ages of the donor tissue in each group. Another limitation worth mentioning is the interval between death and snap freezing: Our previous work[15] did not find any trends in output variables as a function of storage time for up to 3 days of storage in PBS. Girard et al.[37] also found that there was no statistical difference in the mechanical properties of scleral tissue for up to 72 hours storage time. Finally, the SALS technique is inherently destructive, which precludes any additional investigation on the same tissue such as load-dependent microstructure characterization via nondestructive techniques like multiphoton microscopy, a topic of ongoing research in our own laboratory.

In conclusion, although work has been done to characterize the posterior scleral microstructure, this study is the first to quantitatively do so for glaucomatous and nonglaucomatous tissues as a function of both region and depth. The results obtained from this study provide evidence in support of the ongoing hypothesis that microstructural alterations in the posterior human sclera are complex and may occur during the initiation and/or development of glaucoma. Our analysis indicates that region and depth of the posterior sclera are important factors that should be included when one is comparing the scleral microstructure of glaucomatous and nonglaucomatous donor tissue in both experimental and computational work. The dramatic changes observed through the depth of the sclera necessitate that further research include depth as a factor in assessing how observed structural difference may play a role in the development of POAG.

Acknowledgments

The authors thank Mark Borgstrom (Office of Student Computing Resources, University of Arizona) for his statistical support and the Cleveland Eye Bank for the donor tissue.

Supported by American Health Assistance Foundation National Glaucoma Research Grant AHAF G2009035 (JPVG), National Institutes of Health Research Grant 1RO1EY020890-02A1 (JPVG), Research to Prevent Blindness (CAG), partially by the Science Foundation Arizona, and partially by Award No. KUK-C1-013-04 made by King Abdullah University of Science and Technology.

Disclosure: **F.L. Danford**, None; **D. Yan**, None; **R.A. Dreier**, None; **T.M. Cahir**, None; **C.A. Girkin**, None; **J.P. Vande Geest**, None

References

1. Burgoyne CF, Morrison JC. The anatomy and pathophysiology of the optic nerve head in glaucoma. *J Glaucoma*. 2001;10(5 suppl 1):S16–S18.
2. Quigley HA, Addicks EM, Green WR, et al. Optic nerve damage in human glaucoma. II. The site of injury and susceptibility to damage. *Arch Ophthalmol*. 1981;99:635–649.
3. Burgoyne CF, Downs JC, Bellezza AJ, et al. The optic nerve head as a biomechanical structure: a new paradigm for understanding the role of IOP-related stress and strain in the pathophysiology of glaucomatous optic nerve head damage. *Prog Retin Eye Res*. 2005;24:39–73.
4. Hollander H, Makarov F, Stefani FH, et al. Evidence of constriction of optic nerve axons at the lamina cribrosa in the normotensive eye in humans and other mammals. *Ophthalmic Res*. 1995;27:296–309.
5. Quigley HA. Neuronal death in glaucoma. *Prog Retin Eye Res*. 1999;18:39–57.
6. Sigal IA, Flanagan JG, Tertinegg I, et al. Finite element modeling of optic nerve head biomechanics. *Invest Ophthalmol Vis Sci*. 2004;45:4378–4387.
7. Sigal IA, Yang H, Roberts MD, et al. IOP-induced lamina cribrosa displacement and scleral canal expansion: an analysis of factor interactions using parameterized eye-specific models. *Invest Ophthalmol Vis Sci*. 2011;52:1896–1907.
8. Yan DB, Coloma FM, Metheetrairut A, et al. Deformation of the lamina cribrosa by elevated intraocular pressure. *Br J Ophthalmol*. 1994;78:643–648.
9. Burgoyne CF, Downs JC. Premise and prediction-how optic nerve head biomechanics underlies the susceptibility and clinical behavior of the aged optic nerve head. *J Glaucoma*. 2008;17:318–328.
10. Norman RE, Flanagan JG, Sigal IA, et al. Finite element modeling of the human sclera: influence on optic nerve head biomechanics and connections with glaucoma. *Exp Eye Res*. 2011;93:4–12.
11. Girard MJ, Suh JK, Bottlang M, et al. Biomechanical changes in the sclera of monkey eyes exposed to chronic IOP elevations. *Invest Ophthalmol Vis Sci*. 2011;52:5656–5669.
12. Girard MJ, Downs JC, Burgoyne CF, et al. Peripapillary and posterior scleral mechanics–part I: development of an anisotropic hyperelastic constitutive model. *J Biomech Eng*. 2009;131:051011.
13. Girard MJ, Downs JC, Bottlang M, et al. Peripapillary and posterior scleral mechanics–part II: experimental and inverse finite element characterization. *J Biomech Eng*. 2009;131:051012.
14. Watson PG, Young RD. Scleral structure, organisation and disease. A review. *Exp Eye Res*. 2004;78:609–623.
15. Yan D, McPheeters S, Johnson G, et al. Microstructural differences in the human posterior sclera as a function of age and race. *Invest Ophthalmol Vis Sci*. 2011;52:821–829.
16. Pijanka JK, Coudrillier B, Ziegler K, et al. Quantitative mapping of collagen fiber orientation in non-glaucoma and glaucoma posterior human sclerae. *Invest Ophthalmol Vis Sci*. 2012;53:5258–5270.
17. Grytz R, Meschke G. A computational remodeling approach to predict the physiological architecture of the collagen fibril network in corneo-scleral shells. *Biomech Model Mechanobiol*. 2010;9:225–235.
18. Grytz R, Meschke G, Jonas JB. The collagen fibril architecture in the lamina cribrosa and peripapillary sclera predicted by a computational remodeling approach. *Biomech Model Mechanobiol*. 2011;10:371–382.
19. Girard MJ, Dahlmann-Noor A, Rayapureddi S, et al. Quantitative mapping of scleral fiber orientation in normal rat eyes. *Invest Ophthalmol Vis Sci*. 2011;52:9684–9693.
20. Marshall GE, Konstas AG, Lee WR. Collagens in ocular tissues. *Br J Ophthalmol*. 1993;77:515–524.
21. Komai Y, Ushiki T. The three-dimensional organization of collagen fibrils in the human cornea and sclera. *Invest Ophthalmol Vis Sci*. 1991;32:2244–2258.
22. Hernandez MR, Luo XX, Igoe F, et al. Extracellular matrix of the human lamina cribrosa. *Am J Ophthalmol*. 1987;104:567–576.
23. Kokott W. Das spaltlinienbild der sklera (Ein beitrag zum funktionellen bau der sklera). *Klin Monbl Augenheilkd*. 1934;92:177–185.
24. Hogan MJ, Alvarado J, Weddell JE. *Histology of the Human Eye: An Atlas and Textbook*. Philadelphia: WB Saunders; 1971.
25. Winkler M, Jester B, Nien-Shy C, et al. High resolution three-dimensional reconstruction of the collagenous matrix of the human optic nerve head. *Brain Res Bull*. 2010;81:339–348.
26. Sacks MS, Smith DB, Hiester ED. The aortic valve microstructure: effects of transvalvular pressure. *J Biomed Mater Res*. 1998;41:131–141.
27. Sacks MS, Smith DB, Hiester ED. A small angle light scattering device for planar connective tissue microstructural analysis. *Ann Biomed Eng*. 1997;25:678–689.
28. Bettelheim FA, Kumbar M. An interpretation of small-angle lightscattering patterns of human cornea. *Invest Ophthalmol Vis Sci*. 1977;16:233–236.
29. Bettelheim FA, Magrill R. Small-angle light-scattering patterns of corneas of different species. *Invest Ophthalmol Vis Sci*. 1977;16:236–240.
30. Hamann MC, Sacks MS, Malinin TI. Quantification of the collagen fibre architecture of human cranial dura mater. *J Anat*. 1998;192(pt 1):99–106.
31. Keyes JT, Borowicz SM, Rader JH, et al. Design and demonstration of a microbiaxial optomechanical device for multiscale characterization of soft biological tissues with two-photon microscopy. *Microsc Microanal*. 2011;17:167–175.
32. Fazio MA, Grytz R, Bruno L, et al. Regional variations in mechanical strain in the posterior human sclera. *Invest Ophthalmol Vis Sci*. 2012;53:5326–5333.
33. Coudrillier B, Tian J, Alexander S, et al. Biomechanics of the human posterior sclera: age- and glaucoma-related changes measured using inflation testing. *Invest Ophthalmol Vis Sci*. 2012;53:1714–1728.
34. Shaarawy T. *Glaucoma*. Philadelphia: WB Saunders/Elsevier; 2009.
35. Quigley HA. Open-angle glaucoma. *N Engl J Med*. 1993;328:1097–1106.
36. Quigley HA, Addicks EM, Green WR. Optic nerve damage in human glaucoma. III. Quantitative correlation of nerve fiber loss and visual field defect in glaucoma, ischemic neuropathy, papilledema, and toxic neuropathy. *Arch Ophthalmol*. 1982;100:135–146.
37. Girard M, Suh JK, Hart RT, et al. Effects of storage time on the mechanical properties of rabbit peripapillary sclera after enucleation. *Curr Eye Res*. 2007;32:465–470.

Investigative Ophthalmology & Visual Science